Cell Reports

Article

Activity of ventral hippocampal parvalbumin interneurons during anxiety

Graphical abstract

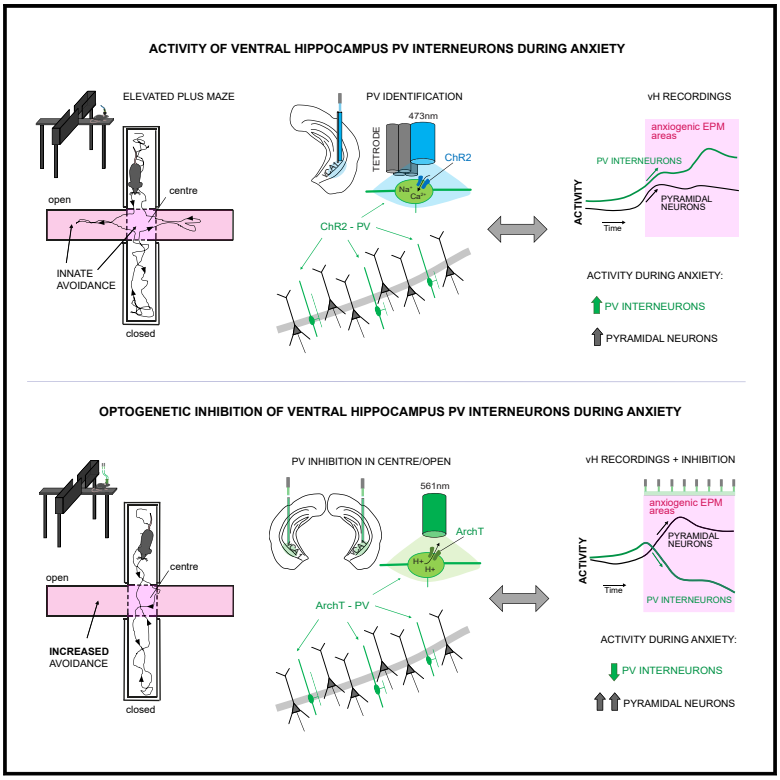

Highlights

- vH PV interneurons are activated in anxiogenic compartments of the EPM
- vH PV interneurons show state-dependent interactions with pyramidal neurons
- vH PV interneurons disinhibit pyramidal neurons in anxiogenic EPM compartments
- Optogenetic inhibition of vH PV interneurons induces persistent anxiety

Authors

Emmanouela Volitaki, Thomas Forro, Kaizhen Li, Thomas Nevian, Stéphane Ciocchi

Correspondence

stephane.ciocchi@unibe.ch

In brief

Volitaki et al. find that inhibitory vH PV interneurons increase their activity in the anxiety-inducing compartments of the elevated plus maze. Optogenetic inhibition of PV interneuron activity in the anxiogenic compartments disinhibits pyramidal neurons and leads to persistent anxiety, suggesting that vH PV interneurons are potential targets for anxiety disorders.

Volitaki et al., 2024, Cell Reports *43*, 114295
June 25, 2024 © 2024 The Author(s). Published by Elsevier Inc.
https://doi.org/10.1016/j.celrep.2024.114295

CellPress

Cell Reports

CellPress
OPEN ACCESS

Article

Activity of ventral hippocampal parvalbumin interneurons during anxiety

Emmanouela Volitaki,[1,3,4] Thomas Forro,[1,4] Kaizhen Li,[1] Thomas Nevian,[2] and Stéphane Ciocchi[1,5,*]
[1]Laboratory of Systems Neuroscience, Department of Physiology, University of Bern, Bühlplatz 5, 3012 Bern, Switzerland
[2]Neuronal Plasticity Group, Department of Physiology, University of Bern, Bühlplatz 5, 3012 Bern, Switzerland
[3]Present address: Friedrich Miescher Institute for Biomedical Research, Fabrikstrasse 24, 4056 Basel, Switzerland
[4]These authors contributed equally
[5]Lead contact
*Correspondence: stephane.ciocchi@unibe.ch
https://doi.org/10.1016/j.celrep.2024.114295

SUMMARY

Anxiety plays a key role in guiding behavior in response to potential threats. Anxiety is mediated by the activation of pyramidal neurons in the ventral hippocampus (vH), whose activity is controlled by GABAergic inhibitory interneurons. However, how different vH interneurons might contribute to anxiety-related processes is unclear. Here, we investigate the role of vH parvalbumin (PV)-expressing interneurons while mice transition from safe to more anxiogenic compartments of the elevated plus maze (EPM). We find that vH PV interneurons increase their activity in anxiogenic EPM compartments concomitant with dynamic changes in inhibitory interactions between PV interneurons and pyramidal neurons. By optogenetically inhibiting PV interneurons, we induce an increase in the activity of vH pyramidal neurons and persistent anxiety. Collectively, our results suggest that vH inhibitory microcircuits may act as a trigger for enduring anxiety states.

INTRODUCTION

Anxiety is an important emotional state that evolved across species to respond to and avoid potential threats.[1,2] However, when the regulation of anxiety is disrupted, this can develop into anxiety disorders, which represent nowadays the most common category of mental disorders.[3] This constitutes a great burden on individual lives and societies that has been further increased by the COVID-19 pandemic[4] and therefore requires a better understanding of the underlying neural mechanism.

Anxiety disorders have been linked to the dysfunction of several neural circuits in brain areas that regulate responses to threatening stimuli, including the amygdala, the prefrontal cortex, and the hippocampus.[5–8] Among these areas, the ventral hippocampus (vH) is a key center that integrates threat-related sensory inputs and forms neuronal representations of emotional contexts to inform executive and decision-making structures to support adaptive behavior.[9–13] Lesions of the vH in rodents or the homologous structure in humans, the anterior hippocampus, result in decreased anxiety levels when facing threatening contexts.[14–16] Moreover, vH hyperactivity in patients and rodent models is associated with increased anxiety levels.[17,18] Therefore, precise control of vH activity is central to regulating anxiety behavior, and this raises the question of which circuit components might be involved. GABAergic interneurons of the vH are in a critical position to modulate neuronal activity through their inhibitory synapses. GABAergic interneurons have been linked to affective disorders,[19] and GABA receptors are binding sites for important anxiolytic drugs such as the benzodiazepines that enhance the effect of GABA onto $GABA_A$ receptors by allosteric modulation.[20] Thus, it has been hypothesized that the disruption of GABAergic circuits could lead to an imbalance of excitation and inhibition and contribute to emotional disorders.[21] However, their role in the control of vH activity during anxiety is largely unknown.

A major population of GABAergic interneurons in the hippocampus is parvalbumin (PV) interneurons.[22,23] These interneurons have been described as fast-spiking, highly active neurons that provide powerful feedback (recurrent and lateral) and feedforward inhibition to different spatial domains of hippocampal pyramidal neurons.[24] The contribution of hippocampal PV interneurons to cognitive functions can be addressed using optogenetic strategies, and previous studies have focused on the function of these interneurons in spatial working memory and social memory.[25,26] Yet, their function in anxiety has not been investigated thus far. In the vH, anxiety has been described to be encoded and driven by pyramidal neurons activated in elevated open compartments of the elevated plus maze (EPM).[11,27] The EPM is a validated anxiety task for rodents that has been used to measure anxiety levels, e.g., under natural conditions or the treatment of anxiolytic drugs.[28–31] During EPM exploration, rodents express innate anxiety about elevated and open spaces by engaging in risk assessment behavior and defensive states that instruct decision-making as the animals leave the closed arms.[32–35]

In this study, we characterized and manipulated the activity of PV interneurons of the vH when mice transitioned from closed (i.e., safer) to open (i.e., more anxiogenic) compartments of the

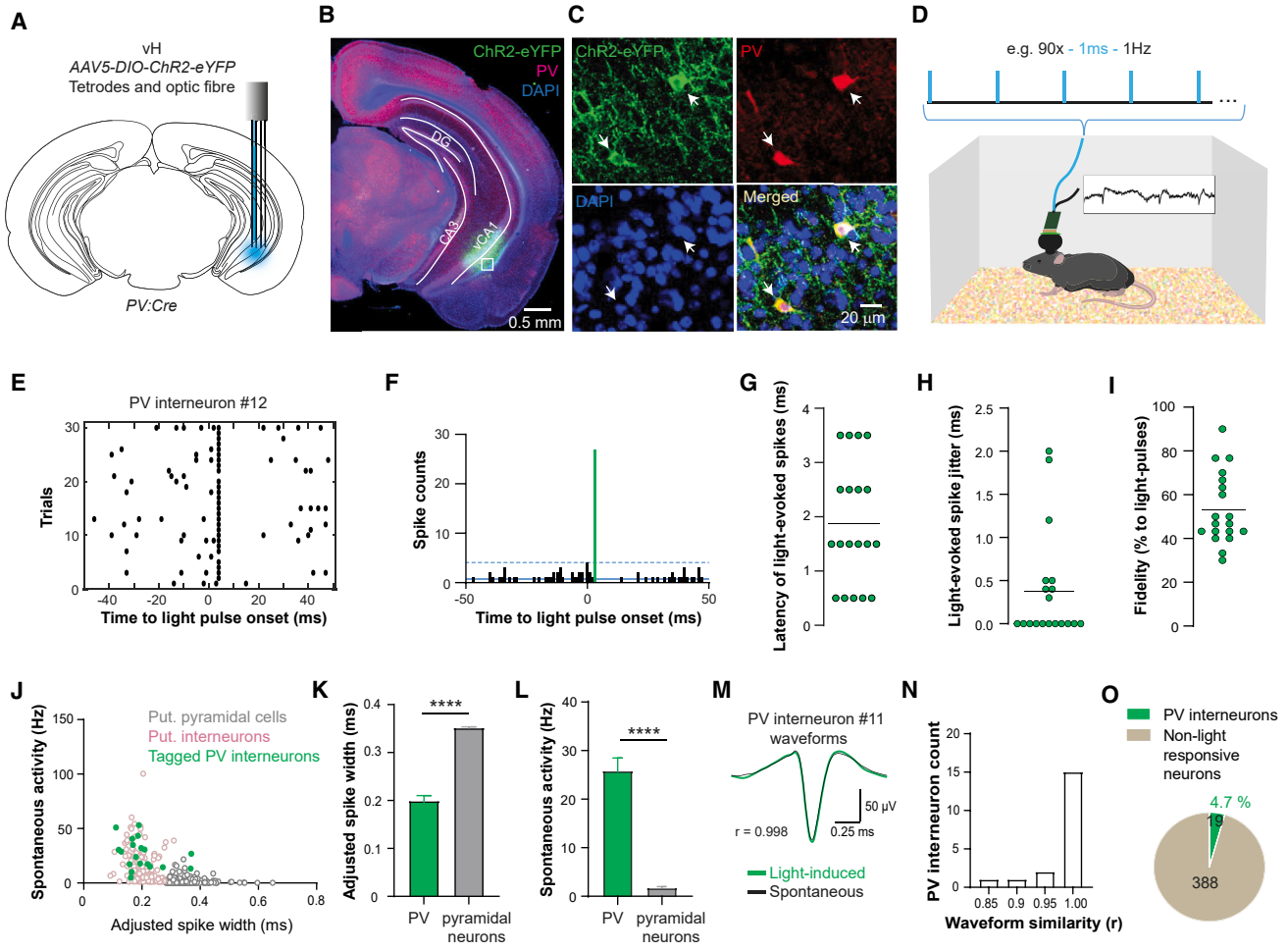

Figure 1. Optogenetic identification of PV interneurons in the vH

(A) Schematic of extracellular single-unit recordings with simultaneous optogenetic stimulation of PV interneurons using tetrode microdrives loaded with optic fibers.

(B) Micrograph of ChR2 expression in PV interneurons in the vH using PV:Cre mice and conditional recombinant adeno-associated virus (rAAV) carrying ChR2. White rectangle includes the region of interest (ROI) magnified in (C).

(C) Close-up micrographs showing PV expression (red) in ChR2-expressing (green) somata confirmed with immunohistochemistry. Arrows point to neurons co-labeled for ChR2-EYFP- and PV-expressing somata.

(D) Schematic of a representative experimental protocol for the photo-tagging of PV interneurons in the homecage. The mice received 90 × 473 nm light pulses of 1 ms duration at 1 Hz while simultaneously recording vH units. For all stimulation protocols, see STAR Methods.

(E) Raster plot of a ventral CA1 hippocampus PV interneuron showing spiking activity 50 ms before and after the light stimulus onset for 30 consecutive trials. Each circle represents one spike.

(F) Peristimulus histogram showing the number of spike counts in (E) in 1 ms bins. In blue: light-evoked neuronal activity. The horizontal solid blue line indicates the average spontaneous activity. The horizontal dashed blue line corresponds to the threshold of neuronal activity, above which the neuronal activity was considered as light evoked.

(G) Latency to light pulses of light-evoked spikes of all identified PV interneurons (n = 19 neurons).

(H) Jitter of light-evoked spikes of all identified PV interneurons (n = 19 neurons).

(I) Fidelity of light-evoked spikes to the 30 randomly selected light pulses (n = 19 neurons).

(J) Spontaneous activity in Hz and adjusted spike width of classified putative pyramidal neurons, putative interneurons (in gray), and optogenetically identified PV interneurons (in light blue) (n = 407 single units).

(K) Comparison of adjusted spike half-width between the PV interneurons and the putative pyramidal neurons. Values are expressed as mean ± SEM. Mann-Whitney U test $p < 0.0001$. PV interneurons median = 0.19 ms, n = 19 neurons; putative pyramidal neurons median = 0.34 ms, n = 230.

(L) Comparison of spontaneous activity between the PV interneurons and the putative pyramidal neurons. Values are expressed as mean ± SEM. Mann-Whitney U test $p < 0.0001$. PV interneurons median = 26.87 Hz, n = 19 neurons; putative pyramidal neurons median = 0.69 Hz, n = 230.

(legend continued on next page)

EPM. Our results showed that PV interneurons exhibit disinhibitory interactions with pyramidal neurons leading to persistent anxiety-related behaviors.

RESULTS

Optogenetic identification of PV interneurons in the vH

We used a photo-tagging approach to identify PV interneurons from vH single-unit recordings in freely moving mice.[36–38] To do so, we implanted optic fibers surrounded by tetrodes in the vH of PV:Cre mice injected with an adeno-associated virus carrying channelrhodopsin-2 (ChR2) and an EYFP cassettes (n = 12 mice, Figures 1A–1C and S1A). The Cre-dependent expression of ChR2 allowed us to selectively photo-excite PV interneurons, and in this way, we optogenetically identified 19 PV interneurons demonstrating short-latency, low-jitter, and high-fidelity responses to light stimulations in the homecage of mice (see STAR Methods; Figures 1D–1I and S2). Based on spike width, spike asymmetry, burst firing, and absolute firing rates, we classified recorded vH single units into putative pyramidal neurons (n = 230) and interneurons (n = 177) and found that the identified PV interneurons displayed narrow-spike shapes and high firing rates, contrasting with pyramidal neurons (Figures 1J–1O).

Activation of PV interneurons upon entry into anxiogenic compartments of the EPM

In line with the anxiogenic nature of open and elevated spaces,[39,40] mice in our experiments spent consistently, across EPM sessions, much less time in the center and open arms of the EPM (Figures 2A, 2B, and S3A).[41–45] However, innate motivation drives rodents to also explore anxiogenic compartments for a potential source of food or for mates,[30] which resulted in entries to the center and the open arm compartments (Figures S3B–S3E). This allowed us to quantify transitions into the center with subsequent transitions to the open arms and investigate how anxiety-related activity and behaviors would change across these transitions on the EPM. Changes in velocity have been suggested to be a predictor of anxiogenesis,[46] and our behavioral analysis on speed revealed that while the mice entered the center from the closed arms, they first slowed down significantly and subsequently further reduced their speed when entering the open arms of the EPM (Figure 2C). In contrast, when mice transitioned from the open arms to the center, they did not show significant changes in speed, but as the mice further moved from the center to closed arms, they strongly increased their speed as they entered the closed arms (Figure 2D). These changes in speed could suggest the perception of anxiogenic components in the EPM center and the open arms as the animals faced openness or were returning to enclosed spaces in the closed arms.

How do PV interneurons respond during these transitions toward more anxiogenic locations? The activity of interneurons and, in particular, PV interneurons in the hippocampus has been described to be correlated with speed,[47,48] and as we observed significant speed changes during transitions between EPM compartments, we fitted a general linear regression model for all neurons analyzed in our study to ensure that we excluded a speed confound on neuronal activity (Figures S3F–S3I).[49] After adjusting for speed, we observed that most PV interneurons (n = 14 out of 19, selection based on a transition activation score; see STAR Methods) gradually increased their activity when the mice approached the center, with a continuous increase in activity upon entrance to the center and open arms (Figure 2E). In contrast, only 3 PV interneurons showed decreasing firing activity as mice entered the center and proceeded to the open compartments (Figure 2F), and 2 PV interneurons showed no change of activation during EPM compartment transitions. The activity of vH pyramidal neurons has been reported to be selectively enhanced in different compartment types of the EPM,[11,49] and in our dataset, we confirmed distinct population responses upon entry to the EPM open compartments. The major population of pyramidal neurons (n = 125) demonstrated an increase in activity in the center or open arms of the EPM, while another population (n = 76) showed a sudden decrease in activity during the same transitions (Figures 2G and 2H). Pyramidal neurons that were selected based only on higher firing rates in the open compared to the closed arms, i.e., "anxiety" cells, already showed increased activity in the EPM center (Figure S4A), suggesting—also on the neuronal level—an increase in anxiogenic representations in the vH. In addition, we analyzed the responses of EPM recorded pyramidal neurons and PV interneurons in another anxiety task, the open field test, which has been shown to induce anxiety-related activity.[27,50] We found that pyramidal neurons that increased their firing during transitions from the periphery to the center of the open field also increased their activity already in the center of the EPM, which was maintained in the open arms (Figures S4B–S4D). In a similar manner, PV interneurons also increased their activity during open field periphery-to-center transitions (Figures S4E and S4F).

We also quantified the response of fast-spiking unidentified interneurons and observed that as a population, they showed similar responses to PV interneurons (Figure S5A). To further elucidate the impact of trajectory types and decisions taken by the animals, we analyzed PV interneuron activity along continuous trajectories taken, navigating from the closed arms to the center to either an open arm or back to a closed arm (Figure S5B). In line with our hypothesis that PV activity is scaling with openness, differences between trajectory-dependent activities appeared only after the EPM center when different compartments were entered. Furthermore, we have

(M) Spike waveform comparison between the spontaneous and light-induced spikes (average of 105 spikes, recorded within 50 ms before light pulse onset, in black compared to average of 170 spikes, recorded within 10 ms after the light-pulse onset, including the light stimulation period, in light blue, respectively) of an optogenetically identified PV interneuron. Pearson's correlation coefficient r = 0.998.

(N) Frequency distribution histogram of Pearson's correlation r values of spontaneous and light-induced spike waveforms of all PV interneurons.

(O) Percentage of photo-tagged PV interneurons out of the total population of recorded neurons (passing the criteria to be classified as putative pyramidal neurons or putative interneurons).

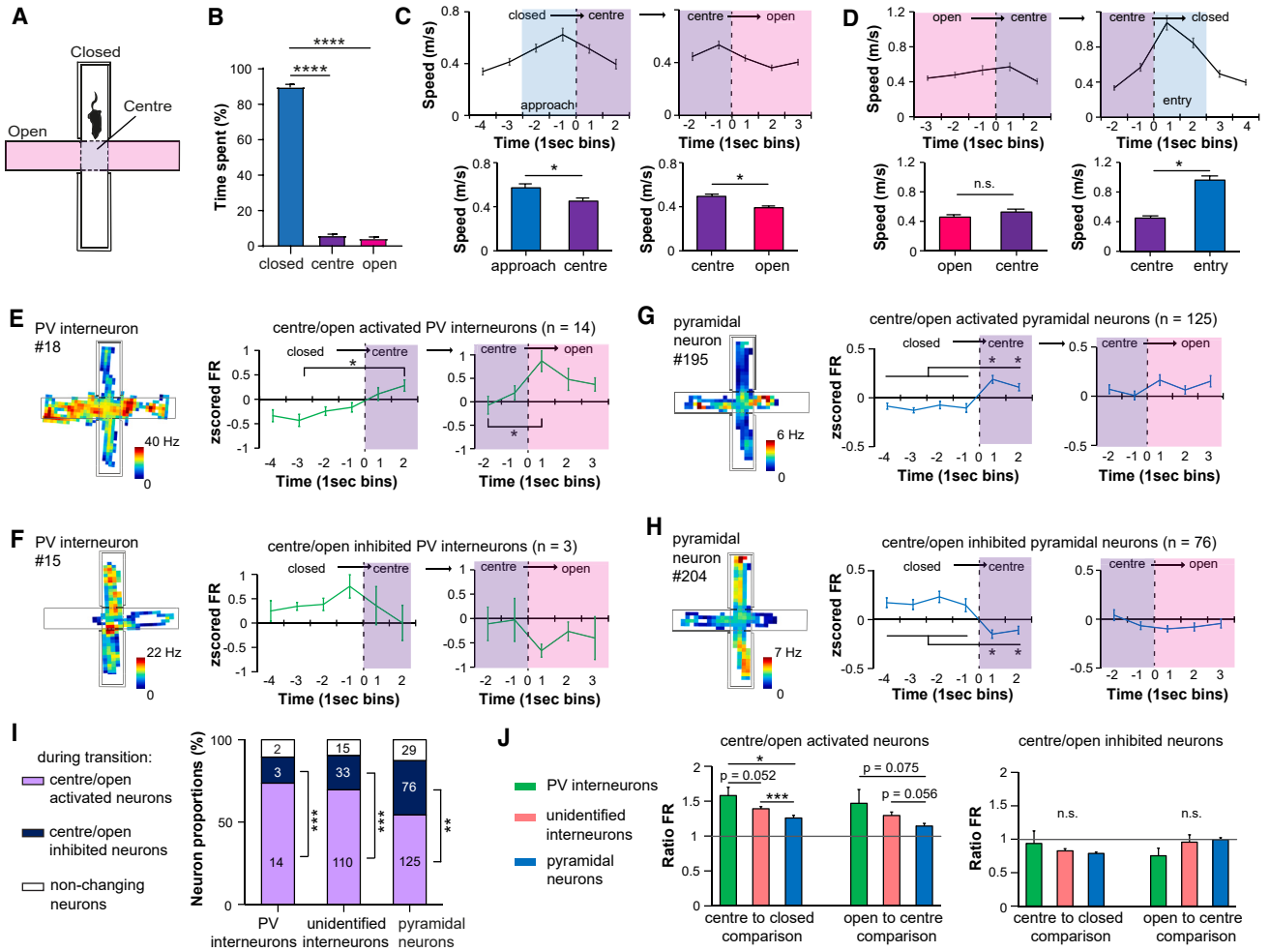

Figure 2. Activation of PV interneurons upon entry into anxiogenic compartments of the EPM

(A) Schematic of the EPM layout with "safe" closed arms, a more anxiogenic center, and open compartments.

(B) The mice spent significantly less time at the center and in the open arms of the EPM. Kruskal-Wallis test $p < 0.001$, Dunn's multiple comparisons test: closed vs. center $p < 0.001$, closed vs. open $p < 0.001$. Number of mice $N = 12$; number of EPM sessions $N = 34$. Error bars represent ± SEM.

(C) Changes in speed of the mice during trajectories approaching the center from the closed arms and transitioning to the center and then further to the open arms. Number of mice = 12; number of EPM sessions = 34. Bottom left, lower average speed when entering the center compared to the approach to the center from the closed arms, 2 s prior to center entry compared to speed during first 2 s of center exploration. Two-tailed Mann-Whitney test $p = 0.0272$. Bottom right, lower average speed when entering the open arms from the center, 2 s before leaving the center compared to 3 s after entering an open arm. Two-tailed Mann-Whitney U test $p = 0.0379$. Error bars represent ± SEM.

(D) Changes in speed of the mice during trajectories approaching the center from the open arms and transitioning to the center and then further to the closed arms. Number of mice = 12; number of EPM sessions = 34. Bottom left, lower average speed when entering the center compared to speed in the open arms. Two-tailed Mann-Whitney test $p = 0.17$. Bottom right, increase of average speed when entering the closed arms from the center (entry defined as the first 2 s in the closed arm). Two-tailed Mann-Whitney U test $p < 0.001$. Error bars represent ± SEM.

(E) Right, spatial heatmap of PV interneuron #18 activity with higher firing rate in the center and open arms of the EPM. Left, population transition activity patterns of center/open activated PV interneurons during trajectories from the closed arms to the center to leaving the center into the open arms. Changes across bins showing a more gradual increase were tested with a one-way repeated ANOVA ($F_{(10,116)} = 5.88$, $p < 0.001$) with Tukey's post hoc multiple comparisons $p < 0.05$. Error bars represent ± SEM.

(F) Right, spatial heatmap of PV interneuron #15 activity with lower firing rate in the center and open arms of the EPM. Left, population transition activity patterns of center/open activated pyramidal neurons during trajectories from the closed arm to the center to leaving the center into the open arms. Changes across bins were tested with a one-way repeated ANOVA ($F_{(10,15)} = 2.09$, $p < 0.09$) with non-significant Tukey's post hoc multiple comparisons. Error bars represent ± SEM.

(G) Right, spatial heatmap of pyramidal neuron #195 activity with higher firing rate in the center and open arms of the EPM. Left, population transition activity patterns of center/open activated pyramidal neurons during trajectories from the closed arm to the center to leaving the center into the open arms. Changes across bins showing a sudden increase were tested with a one-way repeated ANOVA ($F = 8.67_{(10,1074)}$, $p < 0.001$) with Tukey's post hoc multiple comparisons $p < 0.05$. Error bars represent ± SEM.

(legend continued on next page)

analyzed the activity of the different neuronal populations as the mice transitioned from open to closed compartments. We showed that the activity of the anxiety-related neuronal populations is changing in a reverse manner, with subsequent decreases starting in the center and with further decreases of activity in the closed arms (Figures S5C–S5E). This suggests that the activity of these neurons is strongly linked to the EPM compartment identity.

Critically, we found an overrepresentation (i.e., a higher proportion of PV interneurons responding compared to pyramidal neurons) of open compartments among PV interneurons, unidentified interneurons, and pyramidal neurons (Figure 2I) that persisted across EPM sessions (Figures S6F and S6G). Though we observed an overrepresentation in all groups, the magnitude of changes in activity, in particular among PV interneurons but also for unidentified interneurons activated in the open compartments, was greater than that of the corresponding pyramidal neurons (Figure 2J).

Inhibitory interactions between PV interneurons and pyramidal neurons depend on EPM compartments

How might vH PV interneurons interact with and shape the activity of EPM-responsive pyramidal neurons? Feedforward and feedback inhibitory synaptic interactions of PV interneurons with pyramidal neurons in the hippocampus have been described as a mechanism to control local neuronal activity.[24,51–53] As we simultaneously recorded pyramidal neurons with the optogenetically tagged PV interneurons during EPM exploration, and by computing temporal cross-correlation analysis, we observed inhibitory interactions between PV interneurons and pyramidal neurons (Figures 3A–3D). We identified significant short-latency inhibitory interactions in 41 pairs of PV interneurons and pyramidal neurons in the closed compartments of the EPM that were already observed in pre-EPM homecage recording sessions (Figure 3D). When we analyzed the interaction of these pairs in center/open compartments, we detected that inhibitory interactions—with the same spike sampling as in the open compartments—were still significant in the closed arms but not in combined center/open compartments or separately in the open arms or the EPM center (Figures 3E, 3F, and S6, respectively). As the majority of pyramidal neurons inhibited by PV interneurons corresponded to open/center activated neurons (Figure 3G), we hypothesized that, in the closed arms, the activity of pyramidal neurons reflecting anxiety was inhibited by PV interneurons, while in the open arms, disinhibition took place to support anxiety-related firing (Figure 3H).

Optogenetic inhibition of PV interneurons in EPM open compartments induced a lasting increase in the activity of pyramidal neurons leading to persistent anxiety

To further elucidate the contribution of PV interneurons to the activity of pyramidal neurons and anxiety behavior, we optogenetically inhibited PV interneurons in the open or closed compartments of the EPM using conditional expression of ArchT (test group) or tdTomato (control group) in the vH of PV:Cre mice (Figures 4A–4C, S1B, and S1C). Mice first explored the EPM without light application (baseline condition, 5 min). Following this, the mice received continuous light stimulation (561 nm) while they were exploring the open compartments of the EPM (light-on condition, 5 min) and subsequently performed EPM exploration without shining light (light-off condition, 5 min) (Figure 4D). In comparison to the control group, mice expressing ArchT in vH PV interneurons made fewer entries and spent less time in the open arms of the EPM and, most remarkably, in the light-off condition (Figures 4E and S7A). This effect could not be explained by different locomotor activities between the mice groups (Figure 4F). Furthermore, the optogenetic inhibition of PV interneurons induced a lasting increase in the anxiety-related readouts of open compartments that was also observed 24 h later during a follow-up re-exposure to the EPM (Figure 4E). This effect could suggest that there is a long-term plasticity effect of PV interneuron inhibition on anxiety-related behavior. Of note, optogenetic inhibition of PV interneurons in the closed (i.e., safer) arms of the EPM did not impact EPM exploration (Figures S7B and S7C), further pointing to the importance of the activity of PV interneurons during anxiety states.

Which mechanism could underlie persistent anxiety? To address this question, we performed optogenetic inhibition of PV interneurons with simultaneous recordings of vH pyramidal neurons during EPM compartment transitions comparing Arch and EYFP mice (Figures 4G–4I). Interneurons activated during closed-to-center compartment transitions, similar to identified PV interneurons as previously described (Figure 2), were inhibited during the light-on condition in Arch but not EYFP, mice (Figure 4G). Their activity levels recovered in the light-off condition (Figure 4G). Correspondingly, a population of pyramidal neurons was significantly activated in the Arch, but not EYFP, mice in the light-on condition during closed-to-center compartment transitions, suggesting an immediate and temporary disinhibitory effect when PV interneurons were optogenetically inhibited (Figure 4H). Of note, during the light-off condition, we detected an overall higher activity of pyramidal neurons that lasted for several seconds in Arch, but not EYFP, mice while they entered

(H) Right, spatial heatmap of pyramidal neuron #204 activity with lower firing rate in the center and open arms of the EPM. Left, population transition activity patterns of center/open activated pyramidal neurons during trajectories from the closed arm to the center to leaving the center into the open arms. Differences between bins showing a sudden decrease were tested with a one-way repeated ANOVA ($F_{(10,587)} = 9.42$, $p < 0.001$) with Tukey's post hoc multiple comparisons $p < 0.05$. Error bars represent ± SEM.

(I) Proportions of neurons activated or inhibited upon transition into open compartments (including center and open arms) from closed arms based on the measure of an activation score (see STAR Methods). PV interneurons, unidentified interneurons, and pyramidal neurons show an overrepresentation of center/open arm activated neurons compared to center/open inhibited neurons. Chi-squared test, two-sided, $\chi^2 = 12.88$ and $p < 0.001$ for PV interneurons, $\chi^2 = 75.73$ and $p < 0.001$ for unidentified interneurons, and $\chi^2 = 21.22$ and $p < 0.001$ for pyramidal neurons.

(J) Firing rate ratios between EPM compartments during transition trajectories of PV interneurons, unidentified interneurons, and pyramidal neurons. Left, stronger activation of center/open activated PV interneurons and unidentified interneurons than center/open activated pyramidal neurons during closed to center trajectories. Two-tailed Mann-Whitney U test with $p = 0.0142$ and $p < 0.001$. Right, no significant differences across center/open inhibited neurons. Error bars represent ± SEM.

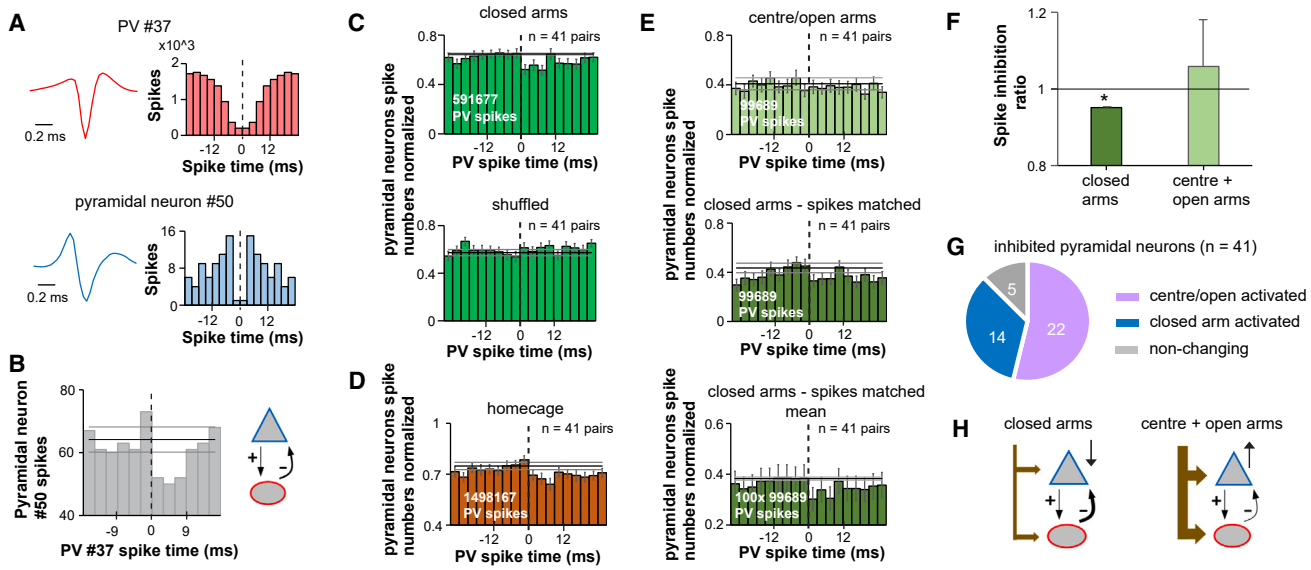

Figure 3. Inhibitory interactions between PV interneurons and pyramidal neurons depend on EPM compartments

(A) Top, average spike waveform and autocorrelogram of PV interneuron #37. Bottom, average spike waveform and autocorrelogram of center/open activated pyramidal neuron #50.

(B) Histogram of pyramidal neuron #50 spike numbers before and after PV interneuron #37 spike times during EPM exploration suggesting reciprocal interactions. Middle black line and 2 gray lines represent mean spike numbers and 98% confidence intervals before the occurrence of PV interneuron spikes, respectively.

(C) Top, average histogram of significant paired interactions between photo-tagged PV interneurons and co-recorded pyramidal neurons with spikes from the closed arms excluding 2 s prior to transition to the center. Significant inhibitory interactions were detected based on lower pyramidal neuron spiking probability after the occurrence of PV interneurons spikes (within 9 ms after) compared to 98% confidence interval of the mean pyramidal spiking probability (15 ms before the PV interneurons spike time occurrence). Bottom, histogram of the same pairs but with the pyramidal spike times shuffled (randomly shifted by 10–50 ms). Error bars represent ± SEM.

(D) Average histogram of pyramidal-PV neuron pairs from the closed arms (see C) quantified in the homecage. Error bars represent ± SEM.

(E) Top, histogram of same pairs as in (C) but in the center + open arms showing reduced inhibitory response of pyramidal neurons. Middle, example histogram of the same pairs in the closed arms but with the same number of spikes as in the center + open arms. Bottom, histogram representing the mean of individual histograms of the same pairs with the same number of spikes as in the center + open arms with 100 times repetition. Error bars represent ± SEM.

(F) Significant inhibition of pyramidal neurons in the closed arms, but not in the center/open arms, comparing 15 ms before and 9 ms after PV interneuron spike occurrence. Wilcoxon signed-rank test against the ratio of 1 (= no change in activity), with $p < 0.001$ in the closed and $p = 0.6726$ in the open arms. Error bars represent ± SEM.

(G) Of the 41 selected pairs of PV interneurons and pyramidal neurons in (C), most pyramidal neurons were activated in the center or open arms during transitions in the EPM.

(H) Model of interactions between PV interneurons and pyramidal neurons in the closed and open arms. In the safe closed arms, there is less anxiety-related input reaching the vH; hence, anxiety neurons are not activated and are further inhibited by PV interneurons. In the more anxiogenic open arms, PV interneurons and pyramidal neurons receive a strong excitatory drive, for example from the amygdala. PV interneurons might be also driven by local pyramidal neurons but show reduced inhibitory interactions (i.e., disinhibition) with pyramidal neurons, resulting in the activation of anxiety neurons.

the open arms of the EPM (Figure 4I). To rule out that a biased sampling of trajectories might be driving the changes in neuronal activities, we compared the underlying number of trajectories taken between Arch and EYFP mice and found that they did not differ in baseline and light-on conditions and saw a trend for less trajectories taken in the light-off condition in Arch mice (possibly driven by changed activity patterns, Figures S8A–S8C). Also, to exclude that by inhibiting PV interneurons, we might have triggered epileptic-like activity that might have contributed to the increased activation, we analyzed the local field potential upon shining light but did not observe any major changes (Figures S8D and S8E).

Based on our findings on state-dependent PV-pyramidal interactions, we further investigated how these interactions would be affected by optogenetic manipulations. By looking at the inhibitory PV-pyramidal pairs, we confirmed the same state-dependent interactions as in previous recordings and showed that after PV inhibition, the inhibitory impact on pyramidal neurons was reduced (Figure S9). Collectively, our findings suggest that temporary optogenetic inhibition of PV interneurons induced a lasting increase in the activity of pyramidal neurons leading to persistent anxiety, possibly via a mechanism involving changed PV-pyramidal synaptic interactions.

DISCUSSION

In our study, we combined optogenetic strategies with single-unit recordings to investigate the contribution of PV interneurons of the vH to anxiety-related behavior. We showed that PV interneurons exhibited an EPM compartment-related change in activity, with the majority of neurons exhibiting increased activity levels in the center and open arms of the EPM. The changes in

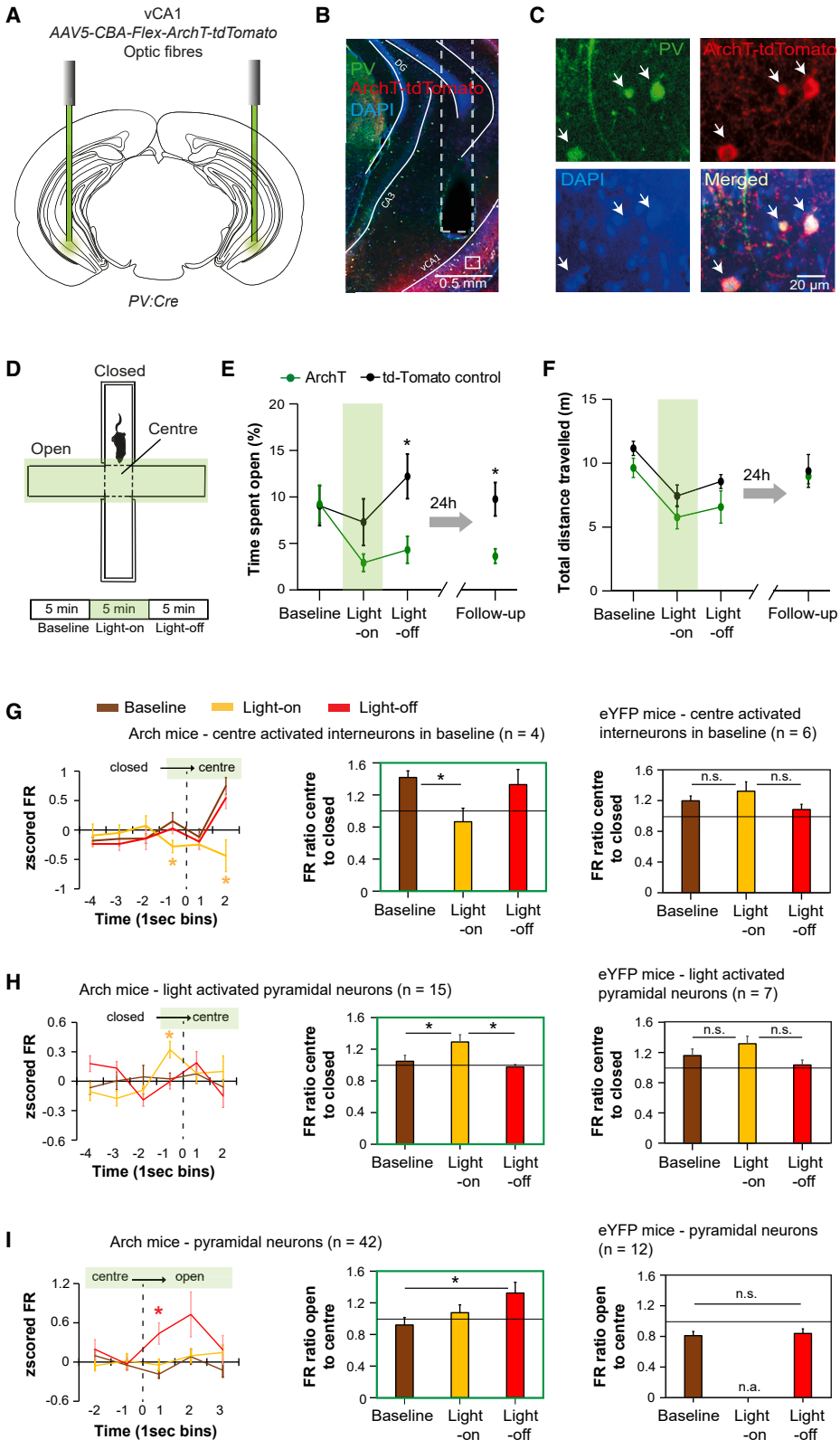

(legend on next page)

the activity of PV interneurons were independent of the trajectories taken and the decisions made (to which compartment the mice would proceed) and translated to the open field test as well. Therefore, we argue that the activity of PV interneurons might be mainly driven by the different anxiogenic encounters of the different EPM compartments.

Our findings further suggest that, in the vH, PV interneurons are activated earlier, more strongly, and uniformly compared to pyramidal neurons during the transitions from the safer to the more anxiogenic compartments of the EPM, indicating that the activity of PV interneurons is not solely driven by local vH pyramidal neuron assemblies during anxiety. Given that PV interneurons showed a similar activation pattern (rather than opposing activation) to pyramidal neurons reflecting anxiety, this raises the question of how these PV interneurons functionally interact at the microcircuit level.

The suppression/inhibition of vH representations has been suggested to be required for anxiolysis.[49,54,55] PV interneurons have been shown to directly inhibit pyramidal neurons,[24,53] an observation we also made in our single-unit recordings using cross-correlation analysis[51] and optogenetic manipulations during anxiety-related behavior. We discovered that the magnitude of inhibitory interactions of PV interneurons onto pyramidal neurons was decreased as the mice entered the center and open compartments of the EPM and that the main targets of PV-interneuron-mediated inhibition corresponded to pyramidal neurons being activated in anxiogenic compartments. Therefore, we showed that PV interneuron recruitment occurs together with a change of inhibitory interactions from safer to more anxiogenic compartments of the EPM, resulting in a net disinhibition of anxiety-related pyramidal neurons and thereby in a parcellation/division of the EPM into different compartments with distinct anxiety contents.

Previous studies have shown that PV interneurons in cortical areas are recruited to specific representations, such as to visual features encoded in the visual cortex, decision-making variables in the prefrontal cortex, or spatial representations in the hippocampus, and that PV interneurons contribute to the tuning of such representations.[38,56,57] We hypothesize that our observations are compatible with such a functional role of PV interneurons whereby they integrate anxiety-related inputs from the basolateral amygdala, ventral CA3 hippocampus, and subpopulations of local pyramidal neurons.[58] In this way, PV interneurons' activity fine-tunes the level of activation and/or assembly selection of anxiety-related information.

Of particular note, the optogenetic inhibition of PV interneurons induced an immediate temporary remapping of some pyramidal neurons that resulted in new, stronger representations of the most anxiogenic compartments of the EPM after light stimulation. Pyramidal neurons representing open compartments have been shown to modulate anxiety levels leading to the avoidance of anxiogenic compartments,[27,59] an observation

Figure 4. Optogenetic inhibition of PV interneurons in EPM open compartments induced a lasting increase in the activity of pyramidal neurons, leading to persistent anxiety

(A) Schematic of bilateral inhibition strategy for vH PV interneurons using implanted optic fibers, rAAV-mediated expression of ArchT in PV:Cre mice.

(B) Micrograph of ArchT-tdTomato expression in the vH in PV interneurons using PV:Cre mice and conditional rAAVs carrying ArchT. White rectangle includes the ROI magnified in (C).

(C) Close-up micrographs showing PV expression (green) in ArchT-tdTomato-expressing somata (red) confirmed with immunohistochemistry.

(D) Schematic of the PV interneuron optogenetic silencing protocol with different conditions on the EPM. The green shaded area corresponds to the light illumination zone.

(E) Avoidance of open arms in ArchT and tdTomato control mice in each condition of the PV interneuron inhibition protocol. ArchT mice significantly decreased their time exploring the open arms after the PV interneuron manipulation and 24 h later in a follow-up test (without light manipulation) compared to the tdTomato controls. Two-way repeated ANOVA, $F_{(2,28)} = 3.4$, and $p = 0.047$ for factor "virus type" including day 1 conditions with post-hoc multiple comparisons (Tukey) $p = 0.0136$ for light off, ArchT mice $N = 8$ and tdTomato mice $N = 8$. For the follow-up with ArchT mice $N = 7$ and tdTomato mice $N = 5$, a two-tailed Mann-Whitney U test was independently applied with $p = 0.0303$. Error bars represent ± SEM.

(F) Distance traveled on the EPM in each condition of the optogenetic inhibition protocol comparing ArchT and tdTomato control mice. Two-way repeated ANOVA, $F_{(2,28)} = 0.08$, and $p = 0.91$ for factor virus type including day 1 conditions with ArchT mice = 8 and tdTomato mice = 8. For the follow-up with ArchT mice $N = 7$ and tdTomato mice $N = 5$, a two-tailed Mann-Whitney U test was applied with $p = 0.75$. Error bars represent ± SEM.

(G) Left, transition-activated interneurons of Arch mice, identified during the baseline condition, showed decreased activity upon light illumination (starting 1 s before entering the center) and a recovery at the light-off condition. Activities were normalized across conditions and compared by shuffling statistics to the baseline condition. Yellow stars mark a significant change in neuronal activity for the light-on condition (shuffling statistics 10,000×, significant probability threshold $p < 0.05$, two-sided). Middle and right, bar graphs of transition-activated interneuron activity expressed as a ratio of center to closed arm activity (bins −1 to 2 s over activity from −4 to −2 s within each stage). Arch group: two-tailed Mann-Whitney U test baseline vs. light-on $p = 0.0317$; EYFP group: two-tailed Mann-Whitney U test baseline vs. light-on $p = 0.24$. Error bars represent ± SEM.

(H) Left, transition-activated pyramidal neuron activity during closed arm-to-center transitions selected from the light-on condition. Activities were normalized across sessions and compared by shuffling statistics to the baseline condition. Yellow stars mark a significant change in neuronal activity for the light-on condition (shuffling statistics 10,000×, significant probability threshold $p < 0.05$, two-sided). Middle and right, bar graphs of transition-activated pyramidal neuron activity expressed as ratio of center activity compared to closed arm activity (bins −1 to 2 s over activity from −4 to −2 s within each stage). Arch group: two-tailed Mann-Whitney U test baseline vs. light-on $p = 0.034$, light-on vs. light-off $p = 0.009$; EYFP group: two-tailed Mann-Whitney U test baseline vs. light-on $p = 0.39$, light-on vs. light-off $p = 0.052$. Error bars represent ± SEM.

(I) Left, total pyramidal neuron population activity during center-to-open arm transitions. The activity showed a significant increase after the entrance to the open arms in the light-off condition. Neuronal activities were normalized across conditions and compared by shuffling statistics to the baseline condition. Red stars mark a significant change in neuronal activity at the light-off condition (shuffling statistics 10,000×, significant probability threshold $p < 0.05$, two-sided). Middle and right, bar graphs of Arch pyramidal neuron activity expressed as ratio of open arm activity compared to center activity (bins 1 to 3 s over activity from −2 to −1 s within each stage) and EYFP pyramidal neurons (12 neurons selected for no open arm activation during baseline for comparability). Arch group: two-tailed Mann-Whitney U test baseline vs. light-off $p = 0.035$; EYFP group: two-tailed Mann-Whitney U test baseline vs. light-on $p = 0.67$. No data are available for the light-on condition for the EYFP group. Error bars represent ± SEM.

corroborated by our data. Moreover, light inhibition of PV interneurons in the closed arms had no behavioral effects on anxiety-related behavior during EPM navigation, suggesting that the effect of PV interneurons is modulatory in an anxiety-state-dependent manner. This is in accordance with our recent study on vH interneurons[49] showing that anxiety-state-dependent interactions were observed in the different EPM compartments in rats with distinct anxiety phenotypes. Such state-dependent interactions might suggest a common principle of action of local vH inhibitory circuits whereby they could contribute to parallel processing[60] and selective routing of information, e.g., anxiety-related activity to the prefrontal cortex and lateral hypothalamus and reward- and goal-related activity to the nucleus accumbens.[11,27,61,62]

The "driving" force for state dependency of anxiety might involve extra-hippocampal inputs (such as from the amygdala) that could set different levels of excitation/membrane potential depolarization levels similar to what has been described for place cell formation.[63] In addition, the state dependency of anxiety might involve changes in inhibitory microcircuit mechanisms through interactions with other interneuron types,[64] as well as inputs and the release of neuromodulators such as dopamine or serotonin in the hippocampus,[65,66] which, by affecting synaptic transmission and plasticity, can impact mnemonic processes.[67] Events that disrupt such mechanisms (such as traumatic events or our optogenetic interference) might result in changes in synaptic plasticity that could potentially imbue memories with altered emotional valence and could explain our findings of persisting anxiety following optogenetic inhibition. This might suggest that PV interneurons could control the transition to long-term forms of anxiety, adding to previous studies implicating PV interneurons in memory-related processes[25,68] and plasticity processes gated by disinhibition.[69] Additionally, we propose and provide evidence that the high activity of PV interneurons during learning of an anxious experience might be required to precisely set the level of pyramidal neuron activation, constraining future behavioral responses to anxiety-inducing situations. Thus, the computations of PV interneurons in the vH could be highly relevant for the development of therapeutic treatments, and modulating their activity during anxiety experiences might affect the transition to persistent forms of anxiety as seen in anxiety disorders.

Limitations of the study

As mice and humans engage in the assessment of open and elevated/high spaces, they evaluate the threat level to inform their decisions for future choices.[70] The vH and its projections to the prefrontal cortex have been shown to be crucial for decision-making during approach-avoidance conflicts.[32,71–75] But the vH's exact role, besides communicating emotionally imbued contexts and memories,[76] in encoding conflict and decisions is not yet well understood.[32] By using the EPM, which is not constituted of clearly externally defined trials (but driven by free exploration), our study cannot fully disentangle cognitive processes (i.e., decision-making) from emotional processes (i.e., anxiety) in the vH. In future experiments using more specific behavioral tasks, one may address whether and how these processes are integrated or represented separately in the vH.

In our study, we targeted PV interneurons, but this population of neurons is comprised of several different cell types such as PV basket, PV bistratified, or PV axo-axonic interneurons.[77] These GABAergic cell types exhibit different dendritic distributions, form synapses with different spatial domains of pyramidal neurons, and are differentially active during network oscillations.[78] Hence, in future studies, it will be important to investigate whether distinct GABAergic cell types differentially contribute to anxiety-related behavior. Moreover, the extent to which GABAergic cell types form functionally uniform populations of neurons recruited to specific assemblies of pyramidal neurons and behaviors is still debated.[51,77,79–82]

STAR★METHODS

Detailed methods are provided in the online version of this paper and include the following:

- KEY RESOURCES TABLE
- RESOURCE AVAILABILITY
  - Lead contact
  - Materials availability
  - Data and code availability
- EXPERIMENTAL MODELS AND SUBJECT DETAILS
- METHOD DETAILS
  - Surgeries and virus injections
  - Histology
  - Behavioral procedures
  - Electrophysiological recordings and data processing
  - Spike classification into putative pyramidal neurons and interneurons
  - Optogenetic identification of PV interneurons
  - EPM transition analysis and functional classification of neurons
- QUANTIFICATION AND STATISTICAL ANALYSIS

SUPPLEMENTAL INFORMATION

Supplemental information can be found online at https://doi.org/10.1016/j.celrep.2024.114295.

ACKNOWLEDGMENTS

This work was supported by the following grants: an ERC starting grant (716761) and a Swiss National Science Foundation professorship grant (170654) (S.C.). We thank Robin Nguyen, Joana Mendes Duarte, and Konstantinos Koukoutselos for help with data processing and histology, Michael Känzig for genotyping the mice, and Christian Dellenbach for technical assistance.

AUTHOR CONTRIBUTIONS

E.V. and S.C. conceived the project and designed experiments. E.V. performed the experiments and collected data. T.F. and E.V. analyzed data with help from S.C. K.L. performed viral injections and procedures for immunolabeling and imaging. S.C., T.F., E.V., K.L., and T.N. contributed to the writing of the manuscript. S.C. and T.N. acquired funding, and S.C. supervised the project.

DECLARATION OF INTERESTS

The authors declare no competing interests.

Received: February 23, 2023
Revised: January 29, 2024
Accepted: May 14, 2024

REFERENCES

1. Steimer, T. (2002). The biology of fear- and anxiety-related behaviors. Dialogues Clin. Neurosci. *4*, 231–249. https://doi.org/10.31887/DCNS.2002.4.3/tsteimer.
2. Barlow, D.H. (2000). Unraveling the mysteries of anxiety and its disorders from the perspective of emotion theory. Am. Psychol. *55*, 1247–1263. https://doi.org/10.1037//0003-066x.55.11.1247.
3. Penninx, B.W., Pine, D.S., Holmes, E.A., and Reif, A. (2021). Anxiety disorders. Lancet *397*, 914–927. https://doi.org/10.1016/S0140-6736(21)00359-7.
4. Santomauro, D.F., Herrera, A.M.M., Shadid, J., Zheng, P., Ashbaugh, C., Pigott, D.M., Abbafati, C., Adolph, C., Amlag, J.O., Aravkin, A.Y., et al. (2021). Global prevalence and burden of depressive and anxiety disorders in 204 countries and territories in 2020 due to the COVID-19 pandemic. Lancet *398*, 1700–1712. https://doi.org/10.1016/S0140-6736(21)02143-7.
5. Quirk, G.J., and Beer, J.S. (2006). Prefrontal involvement in the regulation of emotion: convergence of rat and human studies. Curr. Opin. Neurobiol. *16*, 723–727. https://doi.org/10.1016/j.conb.2006.07.004.
6. Stein, J.L., Wiedholz, L.M., Bassett, D.S., Weinberger, D.R., Zink, C.F., Mattay, V.S., and Meyer-Lindenberg, A. (2007). A validated network of effective amygdala connectivity. Neuroimage *36*, 736–745. https://doi.org/10.1016/j.neuroimage.2007.03.022.
7. Davis, M., and Whalen, P.J. (2001). The amygdala: vigilance and emotion. Mol. Psychiatry *6*, 13–34. https://doi.org/10.1038/sj.mp.4000812.
8. Calhoon, G.G., and Tye, K.M. (2015). Resolving the neural circuits of anxiety. Nat. Neurosci. *18*, 1394–1404. https://doi.org/10.1038/nn.4101.
9. Meyer, H.C., Odriozola, P., Cohodes, E.M., Mandell, J.D., Li, A., Yang, R., Hall, B.S., Haberman, J.T., Zacharek, S.J., Liston, C., et al. (2019). Ventral hippocampus interacts with prelimbic cortex during inhibition of threat response via learned safety in both mice and humans. Proc. Natl. Acad. Sci. USA *116*, 26970–26979. https://doi.org/10.1073/pnas.1910481116.
10. Adhikari, A., Topiwala, M.A., and Gordon, J.A. (2010). Synchronized activity between the ventral hippocampus and the medial prefrontal cortex during anxiety. Neuron *65*, 257–269. https://doi.org/10.1016/j.neuron.2009.12.002.
11. Ciocchi, S., Passecker, J., Malagon-Vina, H., Mikus, N., and Klausberger, T. (2015). Selective information routing by ventral hippocampal CA1 projection neurons. Science *348*, 560–563. https://doi.org/10.1126/science.aaa3245.
12. Felix-Ortiz, A.C., Beyeler, A., Seo, C., Leppla, C.A., Wildes, C.P., and Tye, K.M. (2013). BLA to vHPC inputs modulate anxiety-related behaviors. Neuron *79*, 658–664. https://doi.org/10.1016/j.neuron.2013.06.016.
13. Bannerman, D.M., Rawlins, J.N.P., McHugh, S.B., Deacon, R.M.J., Yee, B.K., Bast, T., Zhang, W.N., Pothuizen, H.H.J., and Feldon, J. (2004). Regional dissociations within the hippocampus–memory and anxiety. Neurosci. Biobehav. Rev. *28*, 273–283. https://doi.org/10.1016/j.neubiorev.2004.03.004.
14. Bannerman, D.M., Grubb, M., Deacon, R.M.J., Yee, B.K., Feldon, J., and Rawlins, J.N.P. (2003). Ventral hippocampal lesions affect anxiety but not spatial learning. Behav. Brain Res. *139*, 197–213. https://doi.org/10.1016/s0166-4328(02)00268-1.
15. Kjelstrup, K.G., Tuvnes, F.A., Steffenach, H.A., Murison, R., Moser, E.I., and Moser, M.B. (2002). Reduced fear expression after lesions of the ventral hippocampus. Proc. Natl. Acad. Sci. USA *99*, 10825–10830. https://doi.org/10.1073/pnas.152112399.
16. Bach, D.R., Guitart-Masip, M., Packard, P.A., Miró, J., Falip, M., Fuentemilla, L., and Dolan, R.J. (2014). Human hippocampus arbitrates approach-avoidance conflict. Curr. Biol. *24*, 541–547. https://doi.org/10.1016/j.cub.2014.01.046.
17. McHugo, M., Talati, P., Armstrong, K., Vandekar, S.N., Blackford, J.U., Woodward, N.D., and Heckers, S. (2019). Hyperactivity and Reduced Activation of Anterior Hippocampus in Early Psychosis. Am. J. Psychiatry *176*, 1030–1038. https://doi.org/10.1176/appi.ajp.2019.19020151.
18. Wolff, A.R., Bygrave, A.M., Sanderson, D.J., Boyden, E.S., Bannerman, D.M., Kullmann, D.M., and Kätzel, D. (2018). Optogenetic induction of the schizophrenia-related endophenotype of ventral hippocampal hyperactivity causes rodent correlates of positive and cognitive symptoms. Sci. Rep. *8*, 12871. https://doi.org/10.1038/s41598-018-31163-5.
19. Grace, A.A. (2010). Ventral Hippocampus, Interneurons, and Schizophrenia: A New Understanding of the Pathophysiology of Schizophrenia and Its Implications for Treatment and Prevention. Curr. Dir. Psychol. Sci. *19*, 232–237. https://doi.org/10.1177/0963721410378032.
20. Barbalho, C.A., Nunes-de-Souza, R.L., and Canto-de-Souza, A. (2009). Similar anxiolytic-like effects following intra-amygdala infusions of benzodiazepine receptor agonist and antagonist: evidence for the release of an endogenous benzodiazepine inverse agonist in mice exposed to elevated plus-maze test. Brain Res. *1267*, 65–76. https://doi.org/10.1016/j.brainres.2009.02.042.
21. Nuss, P. (2015). Anxiety disorders and GABA neurotransmission: a disturbance of modulation. Neuropsychiatr. Dis. Treat. *11*, 165–175. https://doi.org/10.2147/NDT.S58841.
22. Freund, T.F., and Buzsáki, G. (1996). Interneurons of the hippocampus. Hippocampus *6*, 347–470. https://doi.org/10.1002/(SICI)1098-1063(1996)6:4<347::AID-HIPO1>3.0.CO;2-I.
23. Bezaire, M.J., and Soltesz, I. (2013). Quantitative assessment of CA1 local circuits: knowledge base for interneuron-pyramidal cell connectivity. Hippocampus *23*, 751–785. https://doi.org/10.1002/hipo.22141.
24. Hu, H., Gan, J., and Jonas, P. (2014). Interneurons. Fast-spiking, parvalbumin(+) GABAergic interneurons: from cellular design to microcircuit function. Science *345*, 1255263. https://doi.org/10.1126/science.1255263.
25. Deng, X., Gu, L., Sui, N., Guo, J., and Liang, J. (2019). Parvalbumin interneuron in the ventral hippocampus functions as a discriminator in social memory. Proc. Natl. Acad. Sci. USA *116*, 16583–16592. https://doi.org/10.1073/pnas.1819133116.
26. Murray, A.J., Sauer, J.F., Riedel, G., McClure, C., Ansel, L., Cheyne, L., Bartos, M., Wisden, W., and Wulff, P. (2011). Parvalbumin-positive CA1 interneurons are required for spatial working but not for reference memory. Nat. Neurosci. *14*, 297–299. https://doi.org/10.1038/nn.2751.
27. Jimenez, J.C., Su, K., Goldberg, A.R., Luna, V.M., Biane, J.S., Ordek, G., Zhou, P., Ong, S.K., Wright, M.A., Zweifel, L., et al. (2018). Anxiety Cells in a Hippocampal-Hypothalamic Circuit. Neuron *97*, 670–683.e6. https://doi.org/10.1016/j.neuron.2018.01.016.
28. Rodgers, R.J., Cao, B.J., Dalvi, A., and Holmes, A. (1997). Animal models of anxiety: an ethological perspective. Braz. J. Med. Biol. Res. *30*, 289–304. https://doi.org/10.1590/s0100-879x1997000300002.
29. Carobrez, A.P., and Bertoglio, L.J. (2005). Ethological and temporal analyses of anxiety-like behavior: the elevated plus-maze model 20 years on. Neurosci. Biobehav. Rev. *29*, 1193–1205. https://doi.org/10.1016/j.neubiorev.2005.04.017.
30. Cryan, J.F., and Holmes, A. (2005). The ascent of mouse: advances in modelling human depression and anxiety. Nat. Rev. Drug Discov. *4*, 775–790. https://doi.org/10.1038/nrd1825.
31. Walf, A.A., and Frye, C.A. (2007). The use of the elevated plus maze as an assay of anxiety-related behavior in rodents. Nat. Protoc. *2*, 322–328. https://doi.org/10.1038/nprot.2007.44.
32. Ito, R., and Lee, A.C.H. (2016). The role of the hippocampus in approach-avoidance conflict decision-making: Evidence from rodent and human studies. Behav. Brain Res. *313*, 345–357. https://doi.org/10.1016/j.bbr.2016.07.039.
33. Blanchard, D.C., and Meyza, K. (2019). Risk assessment and serotonin: Animal models and human psychopathologies. Behav. Brain Res. *357–358*, 9–17. https://doi.org/10.1016/j.bbr.2017.07.008.
34. Signoret-Genest, J., Schukraft, N., L Reis, S., Segebarth, D., Deisseroth, K., and Tovote, P. (2023). Integrated cardio-behavioral responses to threat

define defensive states. Nat. Neurosci. *26*, 447–457. https://doi.org/10.1038/s41593-022-01252-w.

35. Sestakova, N., Puzserova, A., Kluknavsky, M., and Bernatova, I. (2013). Determination of motor activity and anxiety-related behaviour in rodents: methodological aspects and role of nitric oxide. Interdiscip. Toxicol. *6*, 126–135. https://doi.org/10.2478/intox-2013-0020.

36. Wolff, S.B.E., Gründemann, J., Tovote, P., Krabbe, S., Jacobson, G.A., Müller, C., Herry, C., Ehrlich, I., Friedrich, R.W., Letzkus, J.J., and Lüthi, A. (2014). Amygdala interneuron subtypes control fear learning through disinhibition. Nature *509*, 453–458. https://doi.org/10.1038/nature13258.

37. Kim, D., Jeong, H., Lee, J., Ghim, J.W., Her, E.S., Lee, S.H., and Jung, M.W. (2016). Distinct Roles of Parvalbumin- and Somatostatin-Expressing Interneurons in Working Memory. Neuron *92*, 902–915. https://doi.org/10.1016/j.neuron.2016.09.023.

38. Kvitsiani, D., Ranade, S., Hangya, B., Taniguchi, H., Huang, J.Z., and Kepecs, A. (2013). Distinct behavioural and network correlates of two interneuron types in prefrontal cortex. Nature *498*, 363–366. https://doi.org/10.1038/nature12176.

39. Barnett, S.A. (1975). The Rat : A Study in Behavior, Rev. Edition (University of Chicago Press).

40. Gibson, E.J., and Walk, R.D. (1960). The "visual cliff. Sci. Am. *202*, 64–71.

41. Hernandez-Rapp, J., Smith, P.Y., Filali, M., Goupil, C., Planel, E., Magill, S.T., Goodman, R.H., and Hébert, S.S. (2015). Memory formation and retention are affected in adult miR-132/212 knockout mice. Behav. Brain Res. *287*, 15–26. https://doi.org/10.1016/j.bbr.2015.03.032.

42. Collinson, N., Kuenzi, F.M., Jarolimek, W., Maubach, K.A., Cothliff, R., Sur, C., Smith, A., Otu, F.M., Howell, O., Atack, J.R., et al. (2002). Enhanced learning and memory and altered GABAergic synaptic transmission in mice lacking the alpha 5 subunit of the GABAA receptor. J. Neurosci. *22*, 5572–5580. https://doi.org/10.1523/JNEUROSCI.22-13-05572.2002.

43. Ari C., D'Agostino D.P., Diamond D.M., Kindy M., Park C., Kovacs Z. Elevated Plus Maze Test Combined with Video Tracking Software to Investigate the Anxiolytic Effect of Exogenous Ketogenic Supplements. J. Vis. Exp. 2019;Jan 7:(143). doi:10.3791/58396.

44. Cunniff, M.M., Markenscoff-Papadimitriou, E., Ostrowski, J., Rubenstein, J.L., and Sohal, V.S. (2020). Altered hippocampal-prefrontal communication during anxiety-related avoidance in mice deficient for the autism-associated gene Pogz. Elife *9*, e54835. https://doi.org/10.7554/eLife.54835.

45. Kurilova, E., Sidorova, M., and Tuchina, O. (2023). Single Prolonged Stress Decreases the Level of Adult Hippocampal Neurogenesis in C57BL/6, but Not in House Mice. Curr. Issues Mol. Biol. *45*, 524–537. https://doi.org/10.3390/cimb45010035.

46. Ronquillo, J., Nguyen, M.T., Rothi, L.Y., Bui-Tu, T.D., Yang, J., and Halladay, L.R. (2023). Nature and nurture: Comparing mouse behavior in classic versus revised anxiety-like and social behavioral assays in genetically or environmentally defined groups. Genes Brain Behav. *22*, e12869. https://doi.org/10.1111/gbb.12869.

47. Czurko, A., Huxter, J., Li, Y., Hangya, B., and Muller, R.U. (2011). Theta phase classification of interneurons in the hippocampal formation of freely moving rats. J. Neurosci. *31*, 2938–2947. https://doi.org/10.1523/JNEUROSCI.5037-10.2011.

48. Geiller, T., Vancura, B., Terada, S., Troullinou, E., Chavlis, S., Tsagkatakis, G., Tsakalides, P., Ócsai, K., Poirazi, P., Rózsa, B.J., and Losonczy, A. (2020). Large-Scale 3D Two-Photon Imaging of Molecularly Identified CA1 Interneuron Dynamics in Behaving Mice. Neuron *108*, 968–983.e9. https://doi.org/10.1016/j.neuron.2020.09.013.

49. Forro, T., Volitaki, E., Malagon-Vina, H., Klausberger, T., Nevian, T., and Ciocchi, S. (2022). Anxiety-related activity of ventral hippocampal interneurons. Prog. Neurobiol. *219*, 102368. https://doi.org/10.1016/j.pneurobio.2022.102368.

50. Hale, M.W., Hay-Schmidt, A., Mikkelsen, J.D., Poulsen, B., Shekhar, A., and Lowry, C.A. (2008). Exposure to an open-field arena increases c-Fos expression in a distributed anxiety-related system projecting to the basolateral amygdaloid complex. Neuroscience *155*, 659–672. https://doi.org/10.1016/j.neuroscience.2008.05.054.

51. English, D.F., McKenzie, S., Evans, T., Kim, K., Yoon, E., and Buzsáki, G. (2017). Pyramidal Cell-Interneuron Circuit Architecture and Dynamics in Hippocampal Networks. Neuron *96*, 505–520.e7. https://doi.org/10.1016/j.neuron.2017.09.033.

52. Struber, M., Sauer, J.F., and Bartos, M. (2022). Parvalbumin expressing interneurons control spike-phase coupling of hippocampal cells to theta oscillations. Sci. Rep. *12*, 1362. https://doi.org/10.1038/s41598-022-05004-5.

53. Udakis, M., Pedrosa, V., Chamberlain, S.E.L., Clopath, C., and Mellor, J.R. (2020). Interneuron-specific plasticity at parvalbumin and somatostatin inhibitory synapses onto CA1 pyramidal neurons shapes hippocampal output. Nat. Commun. *11*, 4395. https://doi.org/10.1038/s41467-020-18074-8.

54. Yoshida, K., Drew, M.R., Mimura, M., and Tanaka, K.F. (2019). Serotonin-mediated inhibition of ventral hippocampus is required for sustained goal-directed behavior. Nat. Neurosci. *22*, 770–777. https://doi.org/10.1038/s41593-019-0376-5.

55. Engin, E., Smith, K.S., Gao, Y., Nagy, D., Foster, R.A., Tsvetkov, E., Keist, R., Crestani, F., Fritschy, J.M., Bolshakov, V.Y., et al. (2016). Modulation of anxiety and fear via distinct intrahippocampal circuits. Elife *5*, e14120. https://doi.org/10.7554/eLife.14120.

56. Royer, S., Zemelman, B.V., Losonczy, A., Kim, J., Chance, F., Magee, J.C., and Buzsáki, G. (2012). Control of timing, rate and bursts of hippocampal place cells by dendritic and somatic inhibition. Nat. Neurosci. *15*, 769–775. https://doi.org/10.1038/nn.3077.

57. Runyan, C.A., Schummers, J., Van Wart, A., Kuhlman, S.J., Wilson, N.R., Huang, Z.J., and Sur, M. (2010). Response features of parvalbumin-expressing interneurons suggest precise roles for subtypes of inhibition in visual cortex. Neuron *67*, 847–857. https://doi.org/10.1016/j.neuron.2010.08.006.

58. Lee, S.H., Marchionni, I., Bezaire, M., Varga, C., Danielson, N., Lovett-Barron, M., Losonczy, A., and Soltesz, I. (2014). Parvalbumin-Positive Basket Cells Differentiate among Hippocampal Pyramidal Cells. Neuron *82*, 1129–1144. https://doi.org/10.1016/j.neuron.2014.03.034.

59. Padilla-Coreano, N., Canetta, S., Mikofsky, R.M., Alway, E., Passecker, J., Myroshnychenko, M.V., Garcia-Garcia, A.L., Warren, R., Teboul, E., Blackman, D.R., et al. (2019). Hippocampal-Prefrontal Theta Transmission Regulates Avoidance Behavior. Neuron *104*, 601–610.e4. https://doi.org/10.1016/j.neuron.2019.08.006.

60. Soltesz, I., and Losonczy, A. (2018). CA1 pyramidal cell diversity enabling parallel information processing in the hippocampus. Nat. Neurosci. *21*, 484–493. https://doi.org/10.1038/s41593-018-0118-0.

61. LeGates, T.A., Kvarta, M.D., Tooley, J.R., Francis, T.C., Lobo, M.K., Creed, M.C., and Thompson, S.M. (2018). Reward behaviour is regulated by the strength of hippocampus-nucleus accumbens synapses. Nature *564*, 258–262. https://doi.org/10.1038/s41586-018-0740-8.

62. Pennartz, C.M.A., Ito, R., Verschure, P.F.M.J., Battaglia, F.P., and Robbins, T.W. (2011). The hippocampal-striatal axis in learning, prediction and goal-directed behavior. Trends Neurosci. *34*, 548–559. https://doi.org/10.1016/j.tins.2011.08.001.

63. Mallory, C.S., and Giocomo, L.M. (2018). Heterogeneity in hippocampal place coding. Curr. Opin. Neurobiol. *49*, 158–167. https://doi.org/10.1016/j.conb.2018.02.014.

64. Dudok, B., Klein, P.M., Hwaun, E., Lee, B.R., Yao, Z., Fong, O., Bowler, J.C., Terada, S., Sparks, F.T., Szabo, G.G., et al. (2021). Alternating sources of perisomatic inhibition during behavior. Neuron *109*, 997–1012.e9. https://doi.org/10.1016/j.neuron.2021.01.003.

65. Luchetti, A., Bota, A., Weitemier, A., Mizuta, K., Sato, M., Islam, T., McHugh, T.J., Tashiro, A., and Hayashi, Y. (2020). Two Functionally

Distinct Serotonergic Projections into Hippocampus. J. Neurosci. *40*, 4936–4944. https://doi.org/10.1523/JNEUROSCI.2724-19.2020.

66. Tsetsenis, T., Badyna, J.K., Wilson, J.A., Zhang, X., Krizman, E.N., Subramaniyan, M., Yang, K., Thomas, S.A., and Dani, J.A. (2021). Midbrain dopaminergic innervation of the hippocampus is sufficient to modulate formation of aversive memories. Proc. Natl. Acad. Sci. USA *118*, e2111069118. https://doi.org/10.1073/pnas.2111069118.
67. Wert-Carvajal, C., Reneaux, M., Tchumatchenko, T., and Clopath, C. (2022). Dopamine and serotonin interplay for valence-based spatial learning. Cell Rep. *39*, 110645. https://doi.org/10.1016/j.celrep.2022.110645.
68. Miranda, J.M., Cruz, E., Bessières, B., and Alberini, C.M. (2022). Hippocampal parvalbumin interneurons play a critical role in memory development. Cell Rep. *41*, 111643. https://doi.org/10.1016/j.celrep.2022.111643.
69. Letzkus, J.J., Wolff, S.B.E., Meyer, E.M.M., Tovote, P., Courtin, J., Herry, C., and Lüthi, A. (2011). A disinhibitory microcircuit for associative fear learning in the auditory cortex. Nature *480*, 331–335. https://doi.org/10.1038/nature10674.
70. Biedermann, S.V., Biedermann, D.G., Wenzlaff, F., Kurjak, T., Nouri, S., Auer, M.K., Wiedemann, K., Briken, P., Haaker, J., Lonsdorf, T.B., and Fuss, J. (2017). An elevated plus-maze in mixed reality for studying human anxiety-related behavior. BMC Biol. *15*, 125. https://doi.org/10.1186/s12915-017-0463-6.
71. Bryant, K.G., and Barker, J.M. (2020). Arbitration of Approach-Avoidance Conflict by Ventral Hippocampus. Front. Neurosci. *14*, 615337. https://doi.org/10.3389/fnins.2020.615337.
72. Çavdaroglu, B., Riaz, S., Yeung, E.H.L., Lee, A.C.H., and Ito, R. (2021). The ventral hippocampus is necessary for cue-elicited, but not outcome driven approach-avoidance conflict decisions: a novel operant choice decision-making task. Neuropsychopharmacology *46*, 632–642. https://doi.org/10.1038/s41386-020-00898-z.
73. Yeates, D.C.M., Leavitt, D., Sujanthan, S., Khan, N., Alushaj, D., Lee, A.C.H., and Ito, R. (2022). Parallel ventral hippocampus-lateral septum pathways differentially regulate approach-avoidance conflict. Nat. Commun. *13*, 3349. https://doi.org/10.1038/s41467-022-31082-0.
74. Adhikari, A., Topiwala, M.A., and Gordon, J.A. (2011). Single units in the medial prefrontal cortex with anxiety-related firing patterns are preferentially influenced by ventral hippocampal activity. Neuron *71*, 898–910. https://doi.org/10.1016/j.neuron.2011.07.027.
75. Piquet, R., Faugère, A., and Parkes, S.L. (2024). A hippocampo-cortical pathway detects changes in the validity of an action as a predictor of reward. Curr. Biol. *34*. https://doi.org/10.1016/j.cub.2023.11.036.
76. Nguyen, R., Koukoutselos, K., Forro, T., and Ciocchi, S. (2023). Fear extinction relies on ventral hippocampal safety codes shaped by the amygdala. Sci. Adv. *9*, eadg4881. https://doi.org/10.1126/sciadv.adg4881.
77. Pelkey, K.A., Chittajallu, R., Craig, M.T., Tricoire, L., Wester, J.C., and McBain, C.J. (2017). Hippocampal GABAergic Inhibitory Interneurons. Physiol. Rev. *97*, 1619–1747. https://doi.org/10.1152/physrev.00007.2017.
78. Klausberger, T., and Somogyi, P. (2008). Neuronal diversity and temporal dynamics: the unity of hippocampal circuit operations. Science *321*, 53–57. https://doi.org/10.1126/science.1149381.
79. Maurer, A.P., Cowen, S.L., Burke, S.N., Barnes, C.A., and McNaughton, B.L. (2006). Phase precession in hippocampal interneurons showing strong functional coupling to individual pyramidal cells. J. Neurosci. *26*, 13485–13492. https://doi.org/10.1523/JNEUROSCI.2882-06.2006.
80. Fishell, G., and Kepecs, A. (2020). Interneuron Types as Attractors and Controllers. Annu. Rev. Neurosci. *43*, 1–30. https://doi.org/10.1146/annurev-neuro-070918-050421.
81. Dupret, D., O'Neill, J., and Csicsvari, J. (2013). Dynamic reconfiguration of hippocampal interneuron circuits during spatial learning. Neuron *78*, 166–180. https://doi.org/10.1016/j.neuron.2013.01.033.
82. Buzsaki, G., Geisler, C., Henze, D.A., and Wang, X.J. (2004). Interneuron Diversity series: Circuit complexity and axon wiring economy of cortical interneurons. Trends Neurosci. *27*, 186–193. https://doi.org/10.1016/j.tins.2004.02.007.
83. Hazan L., Zugaro M., and Buzsaki G. Klusters, NeuroScope, NDManager: a free software suite for neurophysiological data processing and visualization. J Neurosci Methods 2006;15:207-216. 10.1016/j.jneumeth.2006.01.017.

STAR★METHODS

KEY RESOURCES TABLE

REAGENT or RESOURCE	SOURCE	IDENTIFIER
Antibodies		
Guinea pig anti-parvalbumin	Synaptic Systems	Cat#195004; RRID: AB_2156476
Rabbit anti-GFP	Abcam	Cat#A11122; RRID: AB_221569
Donkey anti-guinea-pig Alexa Fluor 647	Invitrogen	Cat#A17657; RRID: AB_2340476
Donkey anti-rabbit Alexa Fluor 488	Invitrogen	Cat#R37118; RRID: AB_2556546
Bacterial and Virus Strains		
AAV5.EF1a.DIO.hChR2(E123T/T159C).EYFP.WPRE.hGH	Penn Vector Core	RRID: 35509-AAV5
AAV5-CBA-Flex.ArchT-tdtomato.WPRE.SV40	Penn Vector Core	RRID: 28305-AAV5
AAV-5/2-shortCAG-dlox-tdTomato (rev)-dlox-WPRE-SV40	Viral Vector Facility, Neuroscience Center Zurich	v414-5; RRID: N/A
AAV2/5-EIF1-Flex.Arch3.0-eYFP	Vector Biolabs	Cat#VB4596; RRID: N/A
AAV2/5-EIF1-Flex.eYFP	Vector Biolabs	RRID: 27056-AAV5
Deposited data		
Data and code deposited at Zenodo	Zenodo	https://doi.org/10.5281/zenodo.11108546
Experimental Models: Organisms/Strains		
129P2-Pvalbtm1(cre)Arbr/J (PV-ires Cre)	The Jackson Laboratory	Cat#008069; RRID: IMSR_JAX:008069
Software and Algorithms		
MATLAB	MathWorks	version R2022a
Graphpad Prism	Dotmatics	version 10.2
KlustaKwik, Klusters	Hazan et al.[83]	http://klustakwik.sourceforge.net

RESOURCE AVAILABILITY

Lead contact

Further information and requests for resources and reagents should be directed to and will be fulfilled by the lead contact, Stéphane Ciocchi (stephane.ciocchi@unibe.ch).

Materials availability

This study did not generate new unique reagents.

Data and code availability

- Neurophysiological data underlying the results has been deposited at Zenodo and is publicly available as of the date of publication. DOI is listed in the key resource table.
- All original code has been deposited at Zenodo and is publicly available as of the date of publication. DOI is listed in the key resources table.
- Any additional information required to reanalyze the data reported in this paper is available from the lead contact upon request.

EXPERIMENTAL MODELS AND SUBJECT DETAILS

The data originate from heterozygous male and female PV:Cre mice (The Jackson Laboratory, Bar Harbor, Maine, USA). 12 PV:Cre mice were used for PV interneurons photo-tagging experiments. Behavioral optogenetic experiments were performed with 8 PV:Cre mice (ArchT group) and 8 PV:Cre mice (td-Tomato group) for optogenetic silencing in the open compartments of the EPM. 4 additional mice for ArchT or td-Tomato group were used for optogenetic silencing in the closed arms of the EPM. 4 PV:Cre mice (Arch group) and 4 PV:Cre mice (eYFP group) were used for simultaneous optogenetic stimulation and electrophysiological recordings experiments. Mice were housed individually in a 12 h light/dark cycle throughout the experimental period. Food and water were available *ad libitum* in the homecage, and all behavioral experiments were conducted during the light cycle.

All animal procedures were performed in accordance with the institutional guidelines and were approved by the Veterinary Department of the Canton of Bern.

METHOD DETAILS

Surgeries and virus injections

Mice were anesthetized with isoflurane (Attane, Provet; 5% for induction and 1–1.5% for maintenance) in oxygen-enriched air (VetEquip, KF Technologies) and head-fixed in a stereotactic frame (Kopf Instruments). Intradermal injections of Lidocaine (Lidocain CO_2 20 mg/mL, Sintetica) and subcutaneous injections of Carprofen (5 mg/kg, Rymadil, Zoetis) were administered above the skull for the mice' local anesthesia and analgesia. The mice' body temperature was maintained at 35°C by placing them on a heating pad with feedback control (Harvard Apparatus GmbH).

In order to express the opsins selectively in PV interneurons, conditional Cre-dependent recombinant adeno-associated viruses were injected in the vH CA1 region, following the coordinates AP: −3.08, ML: −3.2 (and +3.2 for the experiments with bilateral PV interneurons inhibition) and DV: −4.2 mm relative to bregma. Specifically for the expression of the excitatory opsin ChR2, 250 nL of AAV5.EF1a.DIO.hChR2(E123T/T159C).EYFP.WPRE.hGH (titer $7x10^{12}$ GC/ml, Penn Vector Core) were injected into the vH CA1 region of PV:Cre knock-in mice. For the expression of the inhibitory proton pump Archaeorhodopsin (Arch) in vH CA1 PV interneurons, we injected 250 nL of AAV5-CBA-Flex.ArchT-tdtomato.WPRE.SV40 ($1.558x10^{13}$ GC/ml, Penn Vector Core) bilaterally (ArchT mice). For the td-Tomato control mice, we injected 250 nL of AAV-5/2-shortCAG-dlox-tdTomato(rev)-dlox-WPRE-SV40 (Viral Vector Facility, University of Zurich) bilaterally. For the expression of Arch unilaterally with simultaneous vH CA1 single unit recordings experiments, Arch mice were injected with 250 nL of AAV5-EIF1-Flex.Arch3.0-eYFP ($1x10^{13}$ GC/ml, Vector Biolabs, Arch mice) and with 250 nL of AAV5-EIF1-Flex.eYFP for the eYFP control mice. rAAVs were delivered to vH CA1 using glass micropipettes (Blaubrand, Brand) with an approximate tip diameter of 40 μm, connected to a picospritzer (Parker Hannifin Corporation).

For the optogenetic inhibition of PV interneurons during EPM navigation, the mice were implanted with custom-made optic fiber implants (diameter: 200 μm, numerical aperture: 0.48, Thorlabs) bilaterally. The tip of each optic fiber was placed 500 μm above the injection site. The optic fiber implants were fixed to the skull with stainless steel screws and resin-based dental cement (A1 Tetric EvoFlow, Ivoclar Vivadent). After the surgery, we waited for at least four weeks to ensure sufficient expression levels of the viral constructs before starting the behavioral experiments.

For the experiments involving optogenetic manipulation with simultaneous vH CA1 single unit recordings, the mice were injected as described above and in the same surgery implanted with custom-made opto-microdrives (Axona Ltd, St. Albans, UK) loaded with 8 independently-moveable tetrodes and 1–2 optic fibers (Thorlabs Inc.Newton, New Jersey, USA). Each tetrode was made of 4 tungsten wires (5 μm inner diameter each, California Fine Wire Company) twisted together. Tetrodes were attached to a connector (Omnetics) with 32 gold pins (Neuralynx) and electroplated to a final impedance of 100–200 kΩ (NanoZ, Multi Channel Systems). Opto-microdrive implants were fixed to the skull with stainless steel screws and resin-based dental cement (A1 Tetric EvoFlow, Ivoclar Vivadent). The total weight of the entire implant did not exceed 3 g. After the surgery, the mice were administered Carprofen (5 mg/kg) for post-operational analgesia and a soft nutrient-enriched paste for food (Omnivore) for 3 days. The mice recovered for at least four weeks to ensure sufficient expression levels of the viral construct before starting the behavioral experiments.

Histology

After completing the behavioral tests, the mice were anesthetized with isoflurane (Attane, Provet; 5% for induction and 2.5% for maintenance) in oxygen-enriched air (VetEquip, KF Technologies). Electrolytic lesions were made at the tip of each recording tetrode by applying a 30 μA current for 10 s. Then the mice were deeply anesthetized with a 5% ketamine (Narketan 10%, Vetoquinol) and 2.5% xylazine (Xylazin, Streuli) solution (0.02 mL/g) and transcardially perfused with phosphate buffer saline (PBS 1:10 dilution from Premixed PBS Buffer 10x, Roche) followed by 4% paraformaldehyde (PFA, Roti Histofix 4%, Roth). The brains were extracted and kept in 4% PFA for 24 h for post-fixation. 70 μm-thick coronal brain slices were cut with a vibratome (VT1000 S, Leica) and preserved in 0.5% sodium azide in PBS at 4°C.

Immunohistochemical reactions were performed in free-floating brain slices to visualise the expression of opsins and reporters. In brief, six brain slices spanning from AP -2.8 to −3.6 mm relative to bregma were used for immunohistochemistry for each mouse. Slices were treated with 0.1% Triton X-100 in PBS (PBS-T) for 5 min and blocked with 5% normal donkey serum (NDS, Abcam) for 30 min in a nutating mixer at room temperature (25°C). The slices were incubated for 72 h at 4°C with an anti-PV antibody raised in guinea pig (1:1000, Synaptic Systems, # 195004) and anti-GFP antibody raised in rabbit (1:1000, Abcam, # A11122), washed with PBST for 5 min (3 repetitions), and incubated again for 2 h with the secondary antibodies: anti-guinea-pig Alexa Fluor 647 and anti-rabbit Alexa Fluor 488 (both 1:1000, raised in donkey, Invitrogen). Slices were mounted on SuperFrost (ThermoFisher) slides and immersed in 4′,6-diamidin-2-phenylindol (DAPI, 1:10000 in PBS) solution for 5 min before adding the mounting medium (AquaPolyMount, Polysciences Inc.) and the coverslip. Slices were imaged using a stereomicroscope (Leica M205 FCA, Leica) mounted with a monochrome camera (Leica DFC345 FX, Leica) and a UV light source (X-CITE, Lumen Dynamics). The position of tetrodes, lesions, optic fiber terminal points and virus expression was determined by examining

the acquired bright field and epifluorescence images. The mice included in the dataset were demonstrating viral expression in vH (unilateral for the *in vivo* optogenetics with single-units experiments; bilateral for the optogenetics only behavioral experiments), the optic fiber tip was between 100 and 500 μm away from vH CA1, and the tetrode terminal points were in vH.

For the animals included in the dataset, brain slices between bregma - 2.8 and −3.8 mm (target region) were imaged on a slide scanning microscope (3dHistech Pannoramic 250 Flash II). The slices, containing the virus injection point were imaged on a confocal laser scanning microscope (Zeiss LSM 880 AxioObserver) with a 20x objective (Plan-Apochromat 20x/0.8 M27) to confirm the co-localisation of PV and opsin-fluorophore.

Behavioral procedures

Elevated plus maze

Before the behavioral experiments, mice were handled through habituation to the experimenter, experimental room and tethering for 1–3 short (10–30 min) sessions. In our study, the mice were tested under three different EPM conditions on the same day: the standard-layout EPM for 10 min under 300 lux. The EPM was custom-made and consisted of four arms, 10 cm wide and 30 cm long, elevated 70 cm above the floor. The two opposing closed arms were enclosed by 18 cm-high walls, whereas the other two were left open. The total number of recording days for each mouse was of a maximum of 4 sessions, with a 3-week break between sessions to keep anxiety levels high (34 sessions, 12 mice, average of 3 sessions per mouse). The mice' head position was tracked using an LED array attached to the headstage with an acquisition rate of 50 frames per second by an overhead video camera (DFK 23FM0-21, ImagingSource).

Open field test

The open field test (OFT) is another behavioral test based on approach-avoidance conflict and consists of a maze in the shape of a square. A subset of animals exposed to the EPM (10/12 animals, 19 OFT experiments, 2 OFT experiments per animal) was subsided to an OFT for 7 min under 50 lux. The OFT arena was a 40 × 40 × 40 cm white cubical platform divided into two zones: the center was defined as the 30 × 30 cm central zone of the OFT arena, and the peripheral zone surrounding the area was defined as the periphery.

Electrophysiological recordings and data processing

The mice recovered for at least 2 weeks before starting the single-unit screening process, during which tetrodes were progressively lowered to the vH CA1 stratum pyramidale using sharp-wave ripples and theta oscillations as electrophysiological hallmarks for the anatomical location of the recorded single-units. Before each recordings during behavioral experiments, the tetrodes were lowered by 50–200 μm to sample new single-units and left in the same position for at least 12 h before starting the recordings during behavior to ensure the stability of the recorded units. The extracellular electrical signals from the tetrodes were amplified, filtered and digitised with a headstage (Intan RHD amplifier, Intan Technologies). The signals were recorded using the RHD recording controller (Intan Technologies) connected to a host computer via a SuperSpeed USB 3.0 cable at 20 kHz. Single units were extracted offline by detecting signal amplitudes 5 SD above the digital filtered signal's root-mean-square (0.8–5 kHz) over 0.2 ms sliding windows. Thirty-two data points (1.6 ms) were sampled for every single unit. A principal component analysis was implemented to extract the first three components of the spike waveforms of each tetrode wire.

Spike waveforms from individual neurons were detected using the KlustaKwik automatic clustering software (http://klustakwik.sourceforge.net/). Individual units were isolated manually by verifying the waveform shape, the modulation of waveform amplitude across tetrode channels, the temporal autocorrelation (to assess the refractory period of a single unit) and cross-correlation (to assess a common refractory period across single units) using Klusters software (Hazan et al., 2006). The stability of single units was confirmed by examining spike features throughout the entire recording.

Spike classification into putative pyramidal neurons and interneurons

The classification of spikes to putative pyramidal neurons and interneurons was performed based on the following parameters[49]: average spike width, shape, firing rate and the 1st moment of autocorrelation (Csicsvari et al., 1998; Riera et al., 2014). An adjusted spike width (adjspkw) for each spike cluster was calculated, incorporating the spike width and spike shape symmetries (Sirota et al., 2008).

$$adjspkw = w * \frac{\left((1+spkScore1)+\left(2-\frac{1}{spkScore2}\right)\right)}{2}$$

w: spike width at 25% from baseline

spkScore1 = peak1 to peak2 difference (=pp) of averaged spike shape normalised. if spkScore1 < 0, spkScore1 = 0

spkScore2 = ratio of trough to peak2 time/peak1 to trough time (tp/pt) of average spike shape, if spkScore2 < 1, spkScore2 = 1.

The adjusted spike width of the recorded neurons showed a bimodal distribution which could be clustered in MATLAB using agglomerative hierarchical clustering. Neurons with an adjusted spike width shorter than 0.28 ms and a firing rate greater than 1 Hz were classified as putative interneurons. In contrast, neurons with an adjusted spike width greater than 0.28 ms and firing rates between 0.05 and 20 Hz were classified as putative pyramidal neurons. Neurons with an adjusted spike width longer than 0.28 ms

and a firing rate higher than 20 Hz were examined for burstiness by calculating the first moment of autocorrelation. Neurons exhibiting their first moment of autocorrelation shorter than 10 ms were classified as bursty pyramidal neurons and neurons with longer than 10 ms fell into the category of wide-spiking interneurons (Fuentealba et al., 2008). Units not fulfilling these criteria (147 out of 554 recorded units, were excluded from the analysis to keep the neuronal classification standards stringent.

Optogenetic identification of PV interneurons

After the completion of the behavioral experiments, the ChR2 mice received 473 nm light pulses of 1 ms and 5 ms duration at frequencies of 1, 10, 20 and 50 Hz in their homecage to activate ChR2 which allowed us to identify on average 2.7 PV interneurons across 7 mice. Spiking activity of interneurons was binned into 1ms bins for time windows of 50 ms before and after the light stimulus onset (time = 0) and for 30 consecutive trials. Single-units were considered as light-responsive if they fulfilled the following criteria: significant spike-timing changes due to light stimulation for a time window 10 ms before and 10 ms after the stimulus onset, using the Stimulus-Associated spike Latency Test (SALT) with $p < 0.001$[38] and a short time-locked response to the stimulation onset (<7 ms).[36]The onset of optogenetically-evoked activity was determined as the activity occurring after the stimulus onset and exceeding the baseline levels by four standard deviations. The time window spanning from the optogenetically-evoked activity until the activity levels return to the baseline levels was defined as the response period of the neuron. The latency was determined as the first time bin after the stimulus onset, during which the activity of the neuron surpasses the four standard deviations from the baseline threshold. The jitter of light-induced spikes was quantified as the standard deviation of light-evoked spikes during the response period. Last, fidelity was calculated as the percentage of light-evoked spikes during the peak response period.

EPM transition analysis and functional classification of neurons

The focus of this study was the analysis of transitions from closed to open compartments of the EPM, reflecting a transition from safer to more anxiogenic compartments. The position of the mice were tracked based on their head positions and the center was manually defined by the experimenter. The mice were considered to have entered a compartment if their head was detected for at least 0.28 s in the compartment. Trajectories were detected when mice navigated from a closed arm into the center where we analyzed the behavior and neuronal activity 4 s before and 2 s after entering the center. We additionally detected trajectories during which mice transitioned from the center to the open arms where we analyzed the behavior and neuronal activity 2 s before leaving the center and 3 s after leaving the center to the open arms. For these trajectories (going from safer to more anxiogenic compartments) we only included trajectories where the center was entered from a closed arm and not an open arm to avoid confounds of anxiety from previous open arm visits. We used these time durations as they reflected the number of trials and time spent in these compartment for reliable data analysis (Figures S3C–S3E). Additionally we detected trajectories in the same manner going the opposite direction from more anxiogenic to safer compartments (open to center to closed).

To classify neurons into different functional groups during transitions, we applied a transition activation score to quantify if a neuron showed activation or inhibition upon entering open compartments:

$$TRscore = \frac{|(\mu open - \mu closed)| - (\sigma\overline{xclosed} + \sigma\overline{xopen})}{\sqrt{3}}$$

μopen: average center or open arm transition activity
μclosed: average closed arm transition activity
σxlcosed: standard error of the mean transition activity in the closed arms
σxopen: standard error of the mean transition activity in the center or open arms.

If the TRscore >0 for either the center or the open arms the neuron was considered as transition-activated or -inhibited depending on whether the average firing in the center or open arms was greater or lower than in the closed arms, respectively.

Open Field transitions were detected with the same analysis with transitions detected to the center not from arms but the periphery and 2 s before and 2 s after center transition. For spatial comparisons, all visits of the periphery were compared to all center visits.

QUANTIFICATION AND STATISTICAL ANALYSIS

Statistical analysis was done in GraphPad PRISM and MATLAB using the Statistics and Machine Learning toolbox and custom scripts. Datasets were tested for normality using the Kolmogorov-Smirnov test. For population samples following the normal distribution, we used parametric tests and for the rest, the equivalent non-parametric tests. Behavioral data of the time spent in EPM compartments were analyzed with the Kruskal-Wallis test (for the EPM PV interneurons photo-tagging experiments) with post hoc Dunn's multiple comparisons tests, and alpha was set to 0.05. To compare the time spent in each EPM compartments between ArchT and td-Tomato mice, we used two-way ANOVA virus and condition as factors and Bonferroni's multiple comparisons post hoc tests, with alpha = 0.05.

Changes in transition activity of neuronal populations were assessed with 1-way ANOVA and Tukey's multiple comparison post hoc tests, with alpha = 0.05. Inhibitory interactions in cross-correlograms were detected if the spiking probability of a pyramidal neuron in either of the 3–9 ms bins after the interneuron spike was below the lower 95% confidence interval limit from the mean spiking probability of 15ms prior the interneuron spike. Differences in the neuronal activity in time bins during transitions between different sessions of simultaneous optogenetic and electrophysiological recordings were tested with shuffling statistics. To do so, the identity of sessions (e.g., baseline vs. light-on) was shuffled and the difference calculated 10000 times. A bin was determined as significantly different if the original difference was greater than 97.5% or lower than 2.5% of the shuffled difference (two-sided statistical test with alpha as 0.05). We used Chi-square tests to compare the proportions of neurons (2-sided, alpha = 0.05).